Nanostructure and Helicity in Syndiotactic Poly(methyl methacrylate) Thermoreversible Gels

Alberto Saiani† and Jean-Michel Guenet*

Laboratoire de Dynamique des Fluides Complexes, Université Louis Pasteur-CNRS UMR 7506, 4, rue Blaise Pascal, F-67070 Strasbourg, France

Received September 21, 1998; Revised Manuscript Received November 24, 1998

ABSTRACT: The structure of thermoreversible gels from syndiotactic poly(methyl methacrylate) has been investigated in two solvents: bromobenzene and toluene. The small-angle neutron scattering experiments can be interpreted by considering a fibrillar nanostructure in which the basic fibrils are double helices of the type put forward recently while the aggregation of three of them generates the junctions. In the wide *q*-range the neutron diffraction data can be theoretically reproduced by considering the same double-helical structure.

Introduction

Highly stereoregular poly(methyl methacrylates), either isotactic (iPMMA) or syndiotactic (sPMMA) or mixtures of isotactic and syndiotactic (stereocomplex), possess the propensity to form thermoreversible gels in a large variety of organic solvents.[1] To throw some light on the mechanism whereby gelation occurs, the level of molecular organization has received considerable attention. In many instances the chain conformation has been described by using double helices. A double intertwined 10_1 helix was suggested for the chain conformation of iPMMA by Kusanagi et al.[2] In gels of a stereocomplex formed from 2:1 mixtures of sPMMA and iPMMA the conformation is also thought to be double-stranded. According to Schomaker and Challa,[3] a 18_1 sPMMA helix wraps around an 9_1 iPMMA helical structure. Fazel et al.[4] have accounted for their small-angle neutron scattering results by considering a fibrillar network in which the basic fibrils are double helices of the type described by Schomaker and Challa while the aggregation of three of them forms the gel junctions.

The structure of sPMMA chains appears to be at variance with those detailed above and has been a matter of debate for the past few years. Kusuyama et al.[5] first proposed a single 74_4 helical model on the basis of X-ray scattering on a solvent-induced crystallized sample. Conversely, Dybal et al.[6] suggested the existence of a double-stranded helical structure from the order of reaction at the early stage of the self-aggregation process of sPMMA gels. This value close to 2 implies the involvement of two chains, but no precise model can be derived. A recent small-angle neutron scattering investigation by Saiani and Guenet[7] has also been shown to be consistent with a double helix in which the inner helix corresponds to the helix proposed by Kusuyama. Unlike the usual double-helix structure, the helix proposed by Saiani and Guenet is, however, asymmetric: the *outer helix is irregular*. This can account for why it has been missed by diffraction experiments while detected by measuring the order of reaction of the aggregation process.

The purpose of this paper is to test further the double-helical model proposed by Saiani and Guenet by means of small-angle neutron scattering on all-labeled gels and by investigating the neutron diffraction range.

Experimental Section

1. Material. The deuterated and the hydrogenated polymers were synthesized in toluene at −78 °C by ion coordination polymerization with triethylaluminum and titanium(IV) chloride as catalysts.[8] In what follows they will be designated as sPMMAD and sPMMAH.

Molecular weight characterization was performed by SEC in THF at 25 °C using the universal calibration method. The following values were obtained:

$$\text{sPMMAH:} \quad M_w = 9.6 \times 10^4 \quad \text{with } M_w/M_n = 1.4$$

$$\text{sPMMAD:} \quad M_w = 1.5 \times 10^5 \quad \text{with } M_w/M_n = 2$$

The tacticity of the hydrogenous polymer was determined in deuterated chloroform by means of proton NMR operating at 200 MHz. The following values were found for the triad arrangements:

$$\text{iso} = 2\%, \quad \text{hetero} = 9\%, \quad \text{syndio} = 89\%$$

Due to the low amount of deuterated material, no NMR investigation was carried out. As the thermal behavior of a 5% gel prepared from the deuterated material exhibited no significant difference compared with that of a hydrogenous polymer, it was accordingly considered that stereoregularity was little altered.

2. Sample Preparation. Samples were prepared directly in sealable quartz cells from HELLMA of optical path of 5 mm for small-angle scattering and in sealable amorphous silica tube of 3 mm inner diameter for neutron diffraction. After sealing from atmosphere appropriate mixtures of the different constituents, the systems were heated close to the solvent boiling point so as to obtain clear, homogeneous solutions. The samples were then quenched at 0 °C for a minimum of 24 h and then aged for 2 weeks at 25 °C.

For the small-angle scattering experiments a series of samples were prepared from hydrogenated polymer and deuterated toluene at four polymer concentrations 2.5%, 5%, 10%, and 15% (v/v). For the diffraction experiments gels at 25% (v/v) were produced from deuterated polymer in either deuterated bromobenzene or toluene.

† Present address: Imperial College, Department of Chemical Engineering, Prince Consort Road, London SW7 2BY UK.

* Corresponding author. Present address: Institut de Chimie des Surfaces et Interfaces, CNRS UPR 9069 BP 2488, 15, rue Jean Starcky, 68057 Mulhouse Cedex, France.

10.1021/ma9814898 CCC: $18.00
Published on Web 01/22/1999

3. Techniques. *(a) Small-Angle Neutron Scattering.* The experiments were carried out on PAXE and PAXY small-angle cameras located at the Laboratoire Léon Brillouin (LLB) (CEN Saclay, France). A wavelength of $\lambda = 0.6$ nm was used with a wavelength distribution characterized by a full width at half-maximum of $\Delta\lambda/\lambda_m = 10\%$. Both cameras possess a two-dimensional sensitive detector composed of 128 × 128 cells. (Further details are available on request at LLB.) By varying the sample−detector distance the available q range was $0.1 < q\ (\mathrm{nm}^{-1}) < 2.5$, with $q = (4\pi/\lambda)\sin(\theta/2)$ where θ is the scattering angle.

Cell efficiency correction was achieved by using the incoherent scattering of hydrogenous *cis*-decalin. The normalized intensity scattered is then written as

$$I_N(q) = \left[\frac{\frac{I_s(q)}{T_s\delta_s} - \frac{I_e(q)}{T_e\delta_e}}{\frac{I_{dec}(q)}{T_{dec}\delta_{dec}} - \frac{I_e(q)}{T_e\delta_e}}\right] \quad (1)$$

in which $I(q)$, δ, and T are the intensity, the thickness, and the transmission, respectively, corresponding to the appropriate subscript to the sample (s), the liquid *cis*-decalin *(*dec), and the empty cell (e).

To extract the coherent intensity scattered by the hydrogenated polymer, we have to subtract the coherent intensity scattered by the solvent and the incoherent intensity scattered by the polymer from the total scattered intensity (the solvents being deuterated their incoherent scattering can be neglected). Fazel et al.[4] have established an experimental relation that allows calculation of the incoherent scattering of the hydrogenous polymer:

$$I_{inc} = 8.65\frac{N_H}{V_H} \quad (2)$$

in which N_H is the number of protons per monomer and V_H the molar volume of the monomer. The absolute coherent intensity scattered by the hydrogenous polymer finally reads

$$I_A(q) = \frac{1}{K}\left[I_N(q) - (1 - C_P)I_D(q) - 8.65C_P\frac{N_H}{V_H}\right] \quad (3)$$

in which $I_D(q)$ is the normalized intensity scattered by the deuterated solvent, C_P the polymer concentration in g/cm^3, and K a calibration constant expressed for PAXE and PAXY as

$$K = \frac{4\pi(a_P - y_{PS}a_S)^2\delta_{dec}T_{dec}N_A}{g(\lambda_m)(1 - T_{dec})m_P{}^2} \quad (4)$$

in which a_P and a_S are the scattering amplitudes of the hydrogenous polymer and the deuterated solvent, y_{PS} is the ratio of their molar volume (V_P/V_S), and m_P is the molecular weight of the polymer monomer unit. $g(\lambda_m)$ is a correction factor which depends on the neutron wavelength λ_m. Here the value of $g(\lambda_m)$ was determined by means of Cotton's method[9] and amounts to

$$g(\lambda_m = 0.6\ \mathrm{nm}) = 1.7 \pm 0.2 \text{ for PAXE}$$

$$g(\lambda_m = 0.6\ \mathrm{nm}) = 1.3 \pm 0.1 \text{ for PAXY}$$

b. Neutron Diffraction. The experiments were carried out on the G6-1 facility located at the Laboratoire Léon Brillouin (LLB) (CEN Saclay, France). G6-1 is a two-axis spectrometer equipped with a banana-type detector made up with 400 cells of angular resolution of 0.2°. A wavelength of $\lambda = 0.474$ nm is obtained by diffraction under Bragg's condition onto a graphite monocrystal. By rotation of the detector, values of q ranging from $2 < q\ (\mathrm{nm}^{-1}) < 25$ were accessible. Cell efficiency correction was achieved with a vanadium sample.

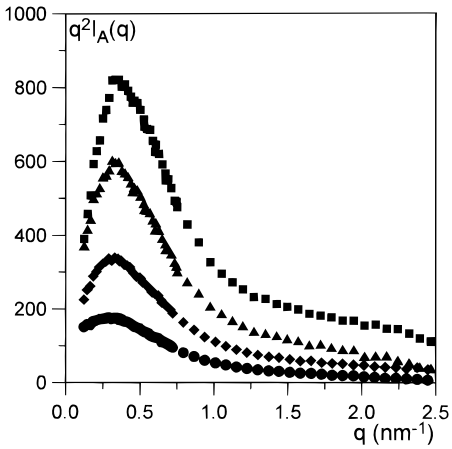

Figure 1. Kratky plot ($q^2I(q)$ vs q) of the intensity scattered by sPMMAH/deuterated toluene gels at different concentrations: 2.5% (●), 5% (◆), 10% (▲), and 15% (■) (v/v). The experiments were carried at room temperature.

To investigate lower q values, some diffraction experiments were performed on D-16, a camera located at the Institut Louis Langevin (ILL) (Grenoble, France). D-16 is equipped with a 64 × 16 wire multidetector which can be turned by 90° around the sample. By reflection on a graphite monochromator a wavelength of $\lambda = 0.45$ nm is selected. The values of q ranged from $q = 1$ nm^{-1} to $q = 6$ nm^{-1}.

The spectra diffracted by pure solvent and by the melted gel were subtracted from the total sample intensity so as to take into account the presence of an amorphous fraction and of free solvent. The fraction of free solvent was calculated on the basis of temperature−concentration phase diagrams reported elsewhere.[10] The fraction of amorphous material was obtained from NMR measurements carried out by Spevacek and co-workers[11,12] on the same type of samples (20% for toluene and 30% for bromobenzene). It is worth emphasizing that this type of subtraction procedure can only provide a semiquantitative analysis. As a matter of fact, cross terms cannot be measured experimentally. Yet, as far as the position of the diffraction maximum is concerned, this approximation has little effect, if any. Only the comparison between calculated and experimental intensities is subject to a lesser accuracy.

Results and Discussion

1. Small-Angle Neutron Scattering. Recent small-angle neutron scattering experiments intended for determining the chain conformation in the gel state of sPMMA have been interpreted with an irregular, asymmetric double helix whose characteristics are as follows:[7]

radius and linear mass of the inner helix:

$$r_1 = 1.1 \pm 0.2\ \mathrm{nm} \qquad \mu_{L1} = 2410 \pm 200\ \mathrm{g/(mol\ nm)}$$

radius and linear mass of the outer helix:

$$r_2 = 2.2 \pm 0.3\ \mathrm{nm} \qquad \mu_{L2} = 1580 \pm 300\ \mathrm{g/(mol\ nm)}$$

Interestingly, the characteristics of the inner helix correspond to the helical conformation already considered by Kusuyama et al.[5]

In these previous experiments only a fraction of the polymer was deuterium-labeled. Here we report additional results gathered on samples where all the polymer chains are labeled with respect to the solvent. We shall therefore attempt to account for the scattering curves by contemplating molecular models where double helices aggregate to form the three-dimensional structure of the gel.

In Figure 1 are shown in a Kratky representation ($q^2I(q)$ vs q) the scattering curves obtained for sPMMAH/deuterated toluene gels at different concentrations. As can be seen, the scattering curves are little dependent upon the concentration effect, especially so for the three highest concentrations (i.e., 5%, 10%, and 15% v/v). In particular, the position of the maximum of the scattering curves does not significantly vary. Only a noticeable discrepancy can be observed for the lowest concentration, i.e., 2.5% (v/v). This concentration is close to the critical gelation concentration ($C_{gel} \approx 1\%$ v/v for sPMMA/toluene gels), and under these conditions the discrepancy is most likely due to the existence of heterogeneities as has been already reported for other systems.[13]

The scattering curves shown here are much reminiscent of results obtained by Fazel et al.[4] for the stereocomplex sPMMA/iPMMA gels. These authors have fitted their results by considering a three-dimensional network in which the fibrils are made up with one double helix and the junctions consist in the aggregation of three double helices. The same type of model can be used here.

In the investigated q range for helical systems only the knowledge of the intensity of the *zeroth*-layer line is relevant so that the scattering reduces to that of infinitely long cylinders:[14]

$$q^2 I_A(q) \propto \pi q \mu_L f(qr) + Cte \qquad (5)$$

in which μ_L is the mass per unit length of the double helix and $f(qr)$ represents the cross-section scattering of the double helix. *Cte* is a constant term taking into account intermolecular scattering. (Although, strictly speaking, this term is not a constant, this approximation holds in the low-q range and is reasonable in the high-q range taking into account the accuracy of the measurements.) For the *zeroth*-layer line, i.e., for $q \leqslant 2\pi/P$, P being the pitch of the helix, $f(qr)$ reads[15]

$$f(qr) = \left[2\frac{r_1 J_1(qr_1) - \gamma_1 r_1 J_1(q\gamma_1 r_1) + r_2 J_1(qr_2) - \gamma_2 r_2 J_1(q\gamma_2 r_2)}{qr_1^2(1-\gamma_1^2) + qr_2^2(1-\gamma_2^2)}\right] \qquad (6)$$

in which r_1 and r_2 are the external radii of the inner and the outer helix, respectively (see Figure 2), and $\gamma_1 = 1 - (e/r_1)$, $\gamma_2 = 1 - (e/r_2)$, e being the thickness of the helices.

The intensity scattered by a parallel aggregation of cylinders has been derived by Oster and Riley[16] and reads

$$q^2 I(q) = \pi q \mu_L \frac{1}{n} f(qr) \sum_{j=1}^{n} \sum_{j \neq k, k=1}^{n} \left[1 + \frac{1}{n} J_0(qr_{jk})\right] \qquad (7)$$

in which n is the number of cylinders and r_{jk} the distance between the axes of the jth and the kth cylinders.

To estimate the intensity scattered by the network portrayed in Figure 3, it is assumed that in the investigated q range the scattering due to the network can be approximated to the scattering by a dilute two-population system of cylinders: the first population consists of the double helices connecting at the junctions and the second population of the junctions themselves (Figure 3).

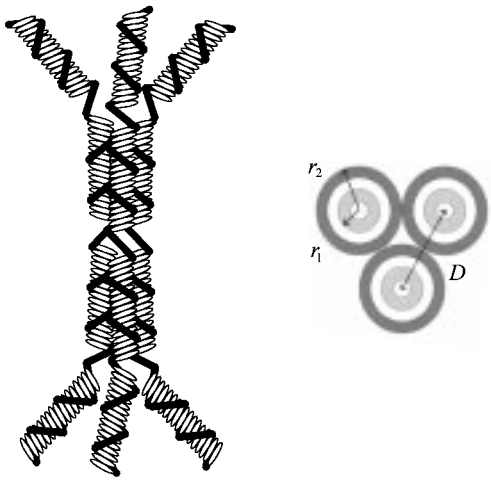

Figure 2. Schematic representation of the network junctions together with their cross section. r_1 and r_2 stand for the inner and the outer helix radius, respectively, and D is the distance between two double helices pertaining to the same junction. The outer helix (black strand) wraps around different inner helices of Kusuyama's type (for details see text).

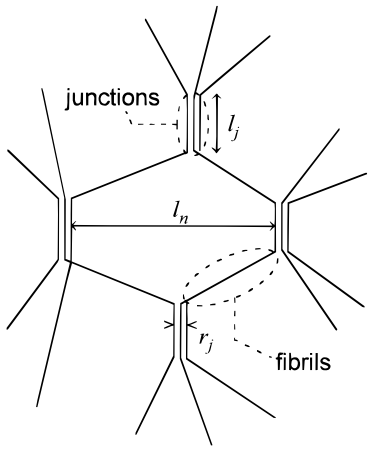

Figure 3. Schematic representation of the network nanostructure l_N is the average mesh size, l_j the average length of the junctions, and r_j their cross-section radius.

This assumption implies that the length of the junctions l_j is far larger than their radius r_j and that the average mesh size of the network l_N is so that $ql_N > 1$. Under these conditions the intensity scattered by this network can be written using eqs 5 and 7:

$$q^2 I_A(q) \propto \pi C_P \mu_L q f(qr)[1 + 2J_0(qD)(1 - B)] \qquad (8)$$

in which C_P is the polymer concentration in g/cm^3, D the distance between the long axes of two adjacent double helices belonging to the same junction (see Figure 2), and B the weight fraction of the junctions. $f(qr)$ is still given by eq 6. Junctions made up from the aggregation of three double helices will be considered. As will be apparent in what follows, junctions with less or more than three double helices cannot account for the data.

It is worth emphasizing that, despite the number of fitting parameters, the uniqueness of the fit is not questionable as each of the parameters has a particular effect on the theoretical curve. The mass per unit length μ_L is directly related to the slope in a Kratky representation and eventually determines the magnitude of the intensity in the whole q range. D determines the cross-

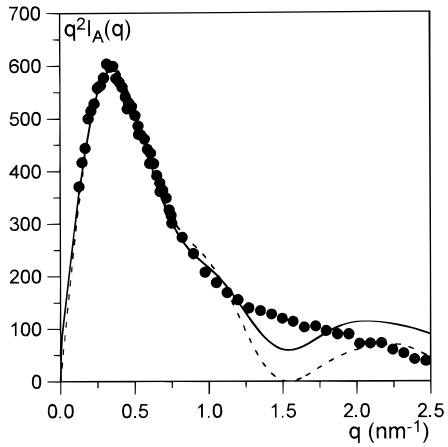

Figure 4. (●) Intensity scattered by a 10% (v/v) sPMMAH/deuterated toluene gel. Solid and dotted lines stand for the best fits (see text for details).

section radius of the second cylinder population; the position of the maximum seen in the Kratky representation sets the value of D. Finally, the value of B allows smoothing of the resulting curve when two populations are considered. There cannot be for, say, a given value of D several possible values of B, and vice versa.

In Figure 4 are drawn by means of a Kratky representation the experimental curve obtained for the 10% (v/v) sPMMA/deuterated toluene gel together with the best fit obtained with the relation 8 by varying D, B, and μ_L, while values obtained previously for the radius of the double helix were used ($r_1 = 1.1 \pm 0.2$ nm, $r_2 = 2.2 \pm 0.3$ nm, and $e = 0.5$ nm). The best fit is obtained for (Figure 4, dotted line)

$$D = 4.9 \pm 0.2 \text{ nm}, \quad B = 0.57 \pm 0.05, \quad \mu_L = 4150 \pm 500 \text{ g/(mol nm)}$$

As can be seen in Figure 4, the theoretical line (dotted line) reproduces fairly well the experimental curve at low q ($q < 1.25$ nm^{-1}). Conversely, for larger q values the theoretical curve displays an oscillation that is not observed experimentally.

Improvement of the fitting procedure can be achieved by introducing a constant term at $q = 0$, of about $q^2I_A(0) \approx 60$, so as to take into account the existence of interactions terms neglected so far. The best fit yields

$$D = 4.6 \pm 0.2 \text{ nm}, \quad B = 0.50 \pm 0.05, \quad \mu_L = 3380 \pm 500 \text{ g/(mol nm)}$$

As can be seen in Figure 4 (full line), the fit is improved in the high-q region, although the oscillation is still present.

Further improvement can be done by taking into account the presence of an amorphous fraction as shown by Spěváček et al. (20% for sPMMA/toluene gels[12]). Assuming that this amorphous fraction behaves Gaussian-like, then its scattering intensity can be calculated from the so-called Debye function:

$$q^2I_A(q) = C_P M_W \frac{2}{q^4 R_G{}^4}[\exp(-q^2 R_G{}^2) + q^2 R_G{}^2 - 1] \quad (9)$$

in which R_G is the mean-square radius of gyration and M_W the weight-averaged molecular weight. Taking $R_G = 10$ nm and $M_W = 100\,000$ g/(mol nm), as derived from previous a study,[7] the same fit as before is obtained (Figure 4, full line) with

$$D = 4.6 \pm 0.2 \text{ nm}, \quad B = 0.49 \pm 0.05, \quad \mu_L = 4260 \pm 500 \text{ g/(mol nm)}$$

The values obtained for D, B, and μ_L through these three different fitting procedures are very close, keeping in mind that the mass per unit length is sensitive to the value of the constant in relation 5. The value obtained for $D \approx 4.6-4.9$ nm, i.e., the distance between adjacent helices in the junction, corresponds to a close packing of double helices in the junction. The fitting procedure and the approximations used appear therefore relevant as self-consistent results are obtained. It has to be notice that D is close to the lattice parameter suggested by Kusuyama et al. ($a = b \approx 4.35$ nm) for crystalline sPMMA samples obtained by exposure to solvent vapors.[5]

The value obtained for the weight fraction of junction is about 50% so that if it is assumed that the junctions have the same length as the double helices connecting at them, then their number fraction is about 16%. Finally, the value of the mass per unit length μ_L of the double helix is in good agreement with the value derived previously.[7]

As stated earlier, an oscillation is observed for $q \approx 2$ nm^{-1} on the theoretical curves which is hardly observed experimentally, except for the 15% sample. Its experimental absence may originate from two effects: (i) the wavelength dispersion on PAXY and PAXE, characterized by a full width at half-maximum of $\Delta\lambda/\lambda_m = 10\%$ and/or (ii) the irregularity of the outer helix of the double-helical form. This problem will be adressed in the next section where it will be shown that the latter effect induces a broadening of the diffraction peaks.

2. Neutron Diffraction. In a previous paper neutron diffraction experiments were shown on sPMMA/toluene and sPMMA/bromobenzene gels. Changing the labeling of the different components (hydrogenated/deuterated) allowed one to show unambiguously the occurrence of polymer/solvent compounds in these systems.[10] In the present paper we shall focus on the structural information that can be extracted from these experiments. For this purpose we will only consider the diffraction curves obtained for fully deuterated samples (i.e., all species are deuterium-labeled).

In Figure 5 are drawn the diffraction curves obtained for a 25% (v/v) sPMMAD/deuterated toluene gel and a 25% (v/v) sPMMAD/deuterated bromobenzene gel on the G-6-1 camera. In the investigated q range five maxima can be clearly observed in both systems at $q_1 \approx 3.7$ nm^{-1}, $q_2 \approx 5.7$ nm^{-1}, $q_3 \approx 7.7$ nm^{-1}, $q_4 \approx 9.4$ nm^{-1}, and $q_5 \approx 12.3$ nm^{-1}. The difference between the relative intensities of the maxima observed for these two systems probably arises from the difference in contrast between the deuterated solvents and the deuterated polymer. In this regard, the maxima in the low-q region are to be quite sensitive to the contrast factor. This will not be taken into consideration herein but is an effect that shall be considered in future studies.

The fit of the diffracted intensity will be presented in two steps for the sake of clarity. As the diffraction q range so that $q > 2\pi/P$, the consideration of several layer lines will be necessary. Equation 8 has been first used, which, as already stated, gives the intensity for the *zeroth*-layer line. The inner and outer radii, r_1 and r_2, were this time used as parameters together with D.

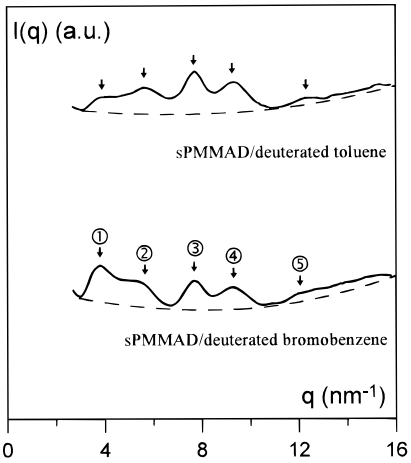

Figure 5. Intensity diffracted by 25% (v/v) sPMMAD/deuterated toluene and sPMMAD/ deuterated bromobenzene gels. In both case five peaks can be clearly identified at $q_1 \approx 3.7$ nm^{-1}, $q_2 \approx 5.7$ nm^{-1}, $q_3 \approx 7.7$ nm^{-1}, $q_4 \approx 9.4$ nm^{-1}, and $q_5 \approx 12.3$ nm^{-1}.

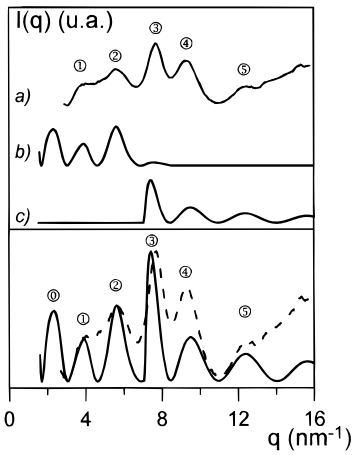

Figure 6. Upper graph: (a) intensity difracted by a 25% (v/v) sPMMAD/deuterated toluene gel, (b) *zeroth-layer line* calculated diffraction by the network, (c) *first-layer line* calculated by considering Kusuyama's helix. Lower graph: (dotted line) intensity diffracted by a 25% (v/v) sPMMAD/deuterated toluene gel; (solid line) sum of the *zeroth-* and *first-layer lines* as calculated above (see text for details).

However, the positions of the maxima are essentially sensitive to r_1 and r_2 and little dependent upon D as is expected. In Figure 6 are drawn the experimental curve obtained for the 25% (v/v) sPMMAD/deuterated toluene gel (curve a) together with the best theoretical curve obtained with relation 8. The following values are obtained:

$$r_1 = 0.95 \pm 0.2 \text{ nm}, \quad r_2 = 2.0 \pm 0.2 \text{ nm}, \quad D = 4.6 \pm 0.3 \text{ nm}$$

The helix radii r_1 and r_2 are in good agreement with those values previously derived from small-angle scattering results,[7] as is the value of D. As was stated above, eq 8 reproduces only the first two maxima at $q_1 \approx 3.7$ nm^{-1} and $q_2 \approx 5.7$ nm^{-1}. Those maxima at high q need consideration of higher diffraction layers.

As we do not know the pitch of the outer helix, the calculation can only be carried out if we consider it to be irregular. In this case, only the regular inner helix will give off diffraction layers. For this reason we shall use the parameters of Kusuyama et al., namely those for a 74_4.[5]

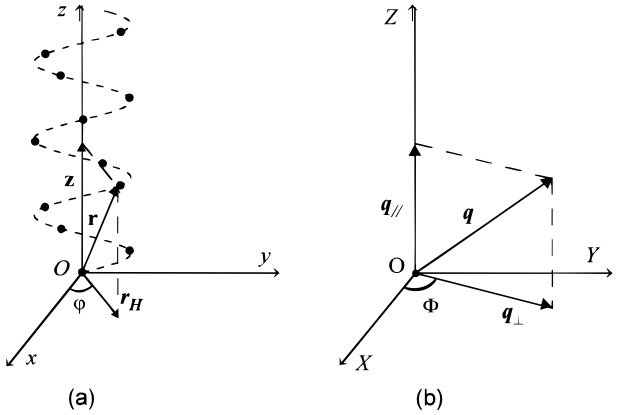

Figure 7. Cylindrical coordinates of a discontinuous helix and the corresponding reciprocal space.

The diffraction layers index of a discontinuous helix made from u basic elements in v turns obey the following selection rule:[17]

$$l = um + vn \tag{10}$$

in which m and n are integers. The fiber period length is $c = vP$, P being, as above, the pitch of the helix. Taking Oz as the helix axis (see Figure 7), then the diffracted intensity is expressed in cylindrical coordinates:[15]

$$F(q_\perp,\Phi,q_{||}) \propto \sum_n^\infty J_n(q_\perp r_H) \exp[in(\Phi + \pi/2)] \tag{11}$$

in which $q_\perp$ and $q_{||}$ are the transfer momenta perpendicular and parrallel to Oz, Φ is an azimutal angle, r_H is the mean radius of the helix, and J_n the Bessel function of first kind and order n. The helix being discontinuous, $q_{||}$ can take on only discrete values corresponding to the diffraction layers: $q_{||} = (2\pi l)/c$. If no particular orientations exist between the helices, then Φ is to be averaged on all its possible values. The diffracted intensity then reads

$$\langle I(q_\perp,(2\pi l)/c)\rangle_\Phi \propto \sum_n^\infty J_n^2(q_\perp r_H) \tag{12}$$

Finally, the intensity can be written for helices without any specific orientation:

$$I(q) \propto \sum_n^\infty J_n^2(qr_H[1 - (2\pi l/qc)^2]^{1/2}) \tag{13}$$

since

$$q^2 = q_\perp^2 + q_{||}^2 \tag{14}$$

The values of n are given by the selection rules (10). In the case of a 74_4 helix the first intense diffraction layer occurs for $m = 0$ and $n = 1$ and corresponds to $l = 4$. In Figure 6 (curve c) is shown the diffracted intensity due to this first-layer line of Kusuyama's helix by using $r_H = 0.85$ nm (the mean radius) and $c = 3.54$ nm, the fiber period given by Kusuyama et al.[5] As can be seen, it is possible to reproduce the three diffraction maxima at $q_3 \approx 7.7$ nm^{-1}, $q_4 \approx 9.4$ nm^{-1}, and $q_5 \approx 12.3$ nm^{-1} by considering only this layer line. Note that the second

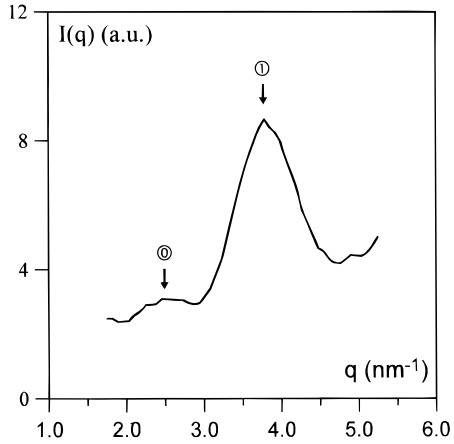

Figure 8. Intensity diffracted by a 25% (v/v) sPMMAD/deuterated toluene gel in a q range accessible through D16 camera. In this q range two peaks can be observed at $q_0 \approx 2.6$ nm^{-1} and $q_1 \approx 3.7$ nm^{-1}. The measurement was carried out at room temperature.

intense layer line would occur for $l = 8$ giving maxima at much higher q values.

Superimposition of the diffracted intensity calculated for the whole double helix for the zeroth-order line together with that calculated for the first intense layer line of Kusuyama's helix gives a theroretical diffraction curve in very good agreement with that measured experimentally (see bottom part of Figure 6). Comparison between experimental and theoretcial curves is achieved by normalizing the zeroth-layer line to the maximum at $q_2 \approx 5.7$ nm^{-1} and first-layer line to the maximum at $q_3 \approx 7.7$ nm^{-1}.

Again, the maximum at $q \sim 2.8$ nm^{-1} is seen on the theoretical curve but is not observed experimentally because out of the G-6-1 detector q range. Clearly, to settle the issue on the existence of the double helix, it is important to find out whether this maximum can effectively be observed experimentally. As a high q resolution is needed, diffraction experiments were again carried out on a 25% (v/v) sPMMAD/deuterated toluene gel on D-16, a camera located at the ILL (Grenoble, France). The results are drawn in Figure 8. The maximum at $q_1 \approx 3.7$ nm^{-1} is again observed together with a maximum $q_0 \approx 2.6$ nm^{-1}, as expected. Oddly enough, the relative intensity of this maximum is rather weak compared to that at $q_1 \approx 3.7$ nm^{-1}. This may arise from a contrast problem as the double helix is suspected to contain solvent molecules occluded between the two single strands.[7,10] Further experiments making use of the deuterium-labeling method are needed to settle this issue.

It is remarkable that the experimental intensity can be reproduced fairly well by considering only these two contributions. This gives strong support to the double-helical structure. Clearly, the first two maxima do not seem to be due to a crystalline lattice but only to Bessel function oscillations due to the helical structure.

The fact that it is not necessary to consider higher diffraction layers of the outer helix strongly points to its irregularity. We suspect that Kusuyama's helix forms first, and then the outer helix wraps around it in an irregular fashion. Interestingly, several authors have already reported a two-step process for the gelation of this polymer, something which may be related to the special double helix.[18,19] It is also worth noting that in all cases the local conformation is *TT* or *near-TT*.

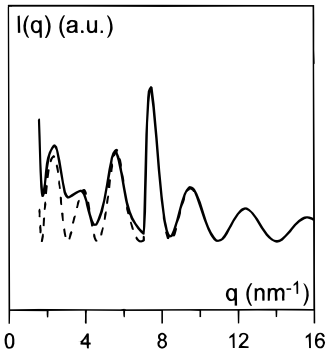

Figure 9. Sum of the *zeroth-layer line* and the *first-layer line* considering this time a radus distribution for the outer helix (see text for details). The dotted line corresponds to the calculation reported in Figure 6.

The irregularity in the wraping process of the outer helix is liable to introduce a radius distribution. This will affect the aspect of the diffraction pattern. Close inspection of the experimental diffraction maxima shows that those attributed to the outer helix look broader and less resolved than those assigned to Kusuyama's helix. In Figure 9 (solid line) is displayed the diffraction curve calculated by introducing a Gaussian radius distribution of full width at half-maximum of 10%. This undoubtedly generates a broadening of the maxima at low q.

Concluding Remarks

The results presented in this paper provide additional support to the double-helical structure of the type proposed by Saiani and Guenet,[7] i.e., a double asymmetric helix where the inner helix is close to the helical form put forward by Kusuyama and co-workers.[5] It is further shown that the gel nanostructure is quite similar to that proposed by Fazel for the stereocomplex gels:[4] the basic fibrils being double helices while the junctions are made up through the aggregation of three basic fibrils. Several authors are now advocating the occurrence of PMMA/solvent compounds;[4,10,20] future studies will have to focus on the role and position of solvent molecules within the helical stucture. This may be the keystone to the understanding of why such an unusual helix can grow.

Acknowledgment. The authors are indebted to A. Brûlet and A. Menelle (LLB) and G. Zaccai (ILL) for experimental assistance.

References and Notes

(1) Spěváček, J.; Schneider, B. *Adv. Colloid Interface Sci.* **1987**, *27*, 81.

(2) Kusunagi, H.; Tadokoro, H.; Chatani, Y. *Macromolecules* **1976**, *9*, 531.

(3) Schomaker, E.; Challa, G. *Macromolecules* **1989**, *22*, 3337.

(4) Fazel, N.; Brûlet, A.; Guenet, J. M. *Macromolecules* **1994**, *27*, 3836.

(5) Kusuyama, H.; Miyamoto, N.; Chatani, Y.; Tadokoro, Y. *Polym. Commun.* **1983**, *24*, 119.

(6) Dybal, G.; Spěváček, J.; Schneider, B. *J. Polym. Sci., Polym. Phys. Ed.* **1986**, *24*, 657.

(7) Saiani, A.; Guenet, J. M. *Macromolecules* **1997**, *30*, 966.

(8) Abe, H.; Imai, K.; Matsumoto M. *J. Polym. Sci., Part C* **1968**, *23*, 469.

(9) Cotton, J. P. In *Neutron, X-ray and light scattering*; Lindner, P., Zemb, T., Eds.; Elsevier: Amsterdam, 1991.

(10) Saiani, A.; Spěváček, J.; Guenet, J. M. *Macromolecules* **1998**, *31*, 703.
(11) Spěváček, J.; Schneider, B.; Bohdanecky, M.; Sikora, A. *J. Polym. Sci., Polym. Phys. Ed.* **1982**, *20*, 1623.
(12) Spěváček, J. Private communication.
(13) See for instance: Guenet, J. M. *Thermorevresible Gelation of Polymers and Biopolymers*; Academic Press: London, 1992.
(14) Pringle, O. A.; Schmidt, P. W. *J. Appl. Crystallogr.* **1971**, *4*, 290.
(15) Porod, G. *Acta Phys. Aust.* **1948**, *2*, 255.
(16) Oster, G.; Riley, D. P. *Acta Crystallogr.* **1952**, *5*, 272.
(17) Cochran, W.; Crick, F. H. C.; Vand, V. *Acta Crystallogr.* **1952**, *5*, 581.
(18) Sedlaček, B.; Spěváček, J.; Mrkvickova, L.; Stejskal, J.; Horska, J.; Baldrian, J.; Quadrat, O. *Macromolecules* **1984**, *17*, 825.
(19) Berghmans, H.; Donkers, A.; Frenay, L.; De Schryver, F. E.; Moldenaers, P.; Mewis, J. *Polymer* **1987**, *28*, 97.
(20) Spěváček, J.; Suchoparek, M. *Macromolecules* **1997**, *30*, 2178.

MA9814898